Int J Adv Manuf Technol (2011) 53:911–919
DOI 10.1007/s00170-010-2890-1

ORIGINAL ARTICLE

Influences of turning parameters in surface residual stresses in AISI 4340 steel

Borja Coto · Virginia García Navas · Oscar Gonzalo · Ana Aranzabe · Carmen Sanz

Received: 23 March 2010 / Accepted: 5 August 2010 / Published online: 24 August 2010

Abstract The study of the residual stresses of parts that work under extreme conditions is of great interest, as they will influence the mechanical behavior of the components. This has a huge importance in the automotive and aeronautics sectors, in components such as power shafts or aircraft landing gears. Machining processes produce thermal and mechanical loads causing residual stresses in the surface of the finished component. The influence of the cutting parameters on the surface residual stresses generated during turning of AISI 4340 (40NiCrMo7) treated steel was analyzed. Surface residual stresses were measured using the X-ray diffraction technique and the $\sin^2\psi$ method. Both magnitude and direction of the residual stresses were assessed in order to understand how the cutting parameters affect the principal stresses directions and the homogeneity of the distribution of stresses. The ANOVA analysis has been used, obtaining the process window to reduce the tensile residual stresses affecting the component behavior against fatigue loads. When feed is increased, more heat is generated during the cutting process, leading to more tensile residual stresses. An increase in cutting speed results in a more adiabatic process (less heating of the part because heat is dissipated through the chip) that also leads to less tensile stresses. It has been observed that the maximum stress is localized around 30° from the cutting direction.

Keywords Residual stress · X-ray diffraction · Turning · AISI 4340 steel

B. Coto (✉) · V. G. Navas · O. Gonzalo · A. Aranzabe · C. Sanz
Fundación Tekniker-IK4.CIC marGUNE,
Avda Otaola, 20,
20600 Eibar, Gipuzkoa, Spain
e-mail: bcoto@tekniker.es

1 Introduction

Residual stresses are those that remain embedded in a body that is not subjected to external loads or thermal gradients. These stresses affect the performance of the final parts, as they influence the fatigue life behavior of components. So, residual stresses must be taken into account in workpieces designed, as the combined effect of internal and applied stress could lead to unexpected failure of a component during its service life. Moreover, residual stresses are considered a key factor in surface integrity of machined parts due to their critical role in component life and corrosion resistance, as discussed by Schwach and Guo [1]. These are the reasons of the increasing interest to know the effects of manufacturing processes on the residual stresses and on the behavior of critical structural components working under extreme conditions.

It is well known that residual stresses arise as a consequence of processing and manufacturing carried out to obtain the final workpieces. In fact, as Withers and Bhadeshia [2] summarize, residual stresses arise in all the manufacturing steps of a component: forming, machining, heat treatment, coating, etc. According to Griffiths [3], and also reported by Wyatt and Berry [4], residual stresses can be formed basically by one of the three following mechanisms: thermal deformation, mechanical deformation, or combined thermal and plastic deformation. In cutting operations, such as turning, the tool-part pressure leads to plastic deformation of the material, and this plastic deformation results in compressive stresses. On the other hand, tool-part friction generates an increase of temperature, and this heat tends to produce tensile stresses in the material, associated to the volume changes that take place when phase transformations occur due to the heating.

Table 1 Chemical composition (wt.%) of AISI 4340 steel (measured experimentally)

	C	Si	Mn	P	S	Cr	Ni	Mo	Fe
wt.%	0.425	0.31	0.81	0.015	0.0058	0.83	1.80	0.25	Balance

Several authors have studied experimentally the influence of some cutting parameters on residual stresses but due to the complexity of residual stress generation, and the high number of parameters influencing the formation of residual stresses, the formulation of a model that is able to predict residual stress taking into account process parameters and material properties is still missing.

Capello [5] analyzed the influence of feed rate, nose radius, depth of cut, and entrance angle on the residual stress generation along the axial direction on different steels, concluding that feed rate and nose radius are the key parameters to control residual stresses in turning. In this case, the cutting speed was not taken into account in the experiments. The influence of the cutting parameters in the principal stresses directions was also not assessed.

Other authors, such as M'Saoubi et al. [6], focused on establishing how mechanical and thermal mechanisms affect the generation of surface residual stress on AISI 316L stainless steel. They analyzed the influence of different cutting parameters, but they found difficult to propose a quantitative interpretation because these effects are interdependent. They analyzed the residual stress along the axial and circumferential directions and observed that circumferential residual stresses are greater than the longitudinal ones.

The same stainless steel was analyzed by Outeiro et al. [7], but again, their assumption of the circumferential and axial directions of turning as the principal stresses directions is not well justified in the case of surface residual stresses as their values for the components of the stress tensor in the machined surface led to changes of the maximum stress directions as the machining regime becomes harder. On the other hand, they found that the circumferential surface residual stresses decreases as cutting speed increases, showing an opposite tendency to the one obtained by other authors such as Jang et al. [8] in AISI 304 stainless steel and Gunnberg et al. [9] in 18MnCr5 low carbon steel, among others.

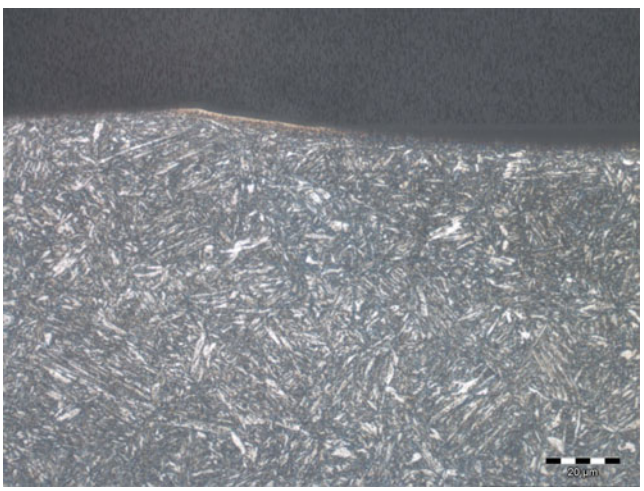

Fig. 1 Microstructure of the AISI 4340 steel used in the work

Summarizing, residual stresses have been analyzed in the longitudinal and/or circumferential directions of turning, but it is not well established that these are the principal stresses directions. The determination of the influence of machining parameters on the principal residual stresses directions has been poorly addressed until now. Moreover, there is a lack of studies supporting that principal stress directions remain without change when changing turning parameters. The analysis and modeling of the influence of machining parameters in the residual stresses will remain incomplete and inaccurate while the assessment of the influence of the machining parameters in the directions of principal residual stresses remains undone. Therefore, the purpose of this work is to analyze the influence of turning parameters on residual stresses, assessing both its magnitude and, what is more important, the direction of the maximum stresses, which is the novelty of present work, as it has not been observed in literature.

2 Material and machining tests

A low alloying AISI 4340 (40NiCrMo7) steel in normalized state was used as work material. This steel is commonly used in the manufacturing of aircraft landing gears, as reported by Pink [10] from BFGoodrich Landing Gear Division.

In Table 1 are gathered the experimentally measured chemical composition of the steel. As this steel is a normal commercial grade, its physical and mechanical properties can be found in bibliography [11, 12]: density=7,700–8,030 kg/m^3; Poisson's ratio=0.30; Elastic Modulus=210 GPa; tensile strength=744.6 MPa; Yield strength=472.3 MPa; etc. A mean hardness of 349 HBW was measured following the standard test UNE-EN ISO 6506-1:2000.

The structure of AISI 4340 is a tempered martensite with sorbe-bainitic appearance. A micrograph of the microstructure can be seen in Fig. 1.

The machining experiments were cylindrical turning conducted in a lathe. An STGCL 2525M16 (ISO code) tool holder was used. A SANDVIK COROMANT tool referenced as TCMT 16T3 08-UF 525M10 was used, which is a tool without coating with M10 hard metal

Table 2 Cutting conditions for turning tests

Parameter	Range
Cutting speed (v_c)	200; 255; 300 m/min
Feed rate (f_n)	0.075; 0.1; 0.125; 0.15; 0.175; 0.2 mm/rev
Depth of cut (a_p)	0.5 mm

quality. It is suitable for a good surface roughness in finishing and light roughing machining of low alloying steels. The final setup has the following characteristics:

- Approach angle (ψr) 91°
- Side rake angle (γf) 0°
- Back rake angle (γp) 0°
- Clearance angle (αf, αp) 7°

A set of cylindrical turning experiments were performed varying cutting speed and feed rate. The range of machining parameters (feed and cutting speed) selected are common cutting conditions in light roughing and finishing cylindrical turning operations for AISI 4340 steel. As some authors [9, 13, 14] state that depth of cut has a negligible influence in the residual stress state, in this work, it was decided to fix the depth of cut. The turning process was performed without cutting fluid. Cutting conditions are summarized in Table 2.

3 Residual stress measurements

The residual stresses in the samples were measured using X-ray diffraction (XRD). The $\sin^2\psi$ method has been used to obtain residual stresses from X-ray diffraction measurements.

Residual stress measurement with XRD is based on measuring the strain and then calculating the stress using the elasticity theory. The strain can be obtained from the variation in lattice spacing that, according to Bragg law ($\lambda = 2 \cdot d \cdot \sin\theta$), is reflected in a change in the diffraction peak position:

$$\varepsilon = \frac{d - d_0}{d_0} = \frac{\sin\theta_0}{\sin\theta} - 1 \tag{1}$$

The $\sin^2\psi$ method, described by Lu [15] and Noyan and Cohen [16], is a well established and widely accepted residual stress calculation method. Due to the low penetration of X-rays in the material, a plane stress model can be assumed and then the strain in a direction defined by ϕ and ψ angles can be expressed as a function of the stress components (σ_{ij}):

$$\varepsilon_{\phi\psi} = \frac{1}{2}s_2\sigma_\phi \sin^2\psi + s_1[\sigma_{11} + \sigma_{22}] + \frac{1}{2}s_2\sigma_{\text{shear}} \sin 2\psi \tag{2}$$

where σ_ϕ is the residual stress along the ϕ direction defined in the sample reference system, and σ_{shear} holds the information about shear stresses. These normal and shear stresses are related to the stress tensor components, σ_{ij}, as follows:

$$\sigma_\phi = \sigma_{11}\cos^2\phi + \sigma_{12}\sin 2\phi + \sigma_{22}\sin^2\phi \tag{3}$$

$$\sigma_{\text{shear}} = \sigma_{13}\cos\phi + \sigma_{23}\sin\phi \tag{4}$$

In Eq. (2), s_1 and $1/2s_2$ are the defined as

$$s_1 = -\frac{\nu}{E} \tag{5}$$

$$\frac{1}{2}s_2 = \frac{\nu + 1}{E} \tag{6}$$

where ν is the Poisson's ratio and E is the Young's modulus of the material. These are the elastic constants for the crystallographic direction perpendicular to the lattice planes where the strain is measured (planes defined by the Miller indices (hkl)). These elastic constants differ from the bulk ones, which are an average over all directions in the crystal lattice, because of elastic anisotropy.

In the present work, a Bruker D8 Advance X-ray diffractometer equipped with Cr radiation ($\lambda_{k\alpha}$=2.291 Å) and parallel beam was used to perform the residual stress measurements. The (hkl)=(211) reflection, corresponding to a peak around 2θ=156° has been used. Table 3 summarizes the conditions used for the X-ray diffraction measurements. A sliding gravity method was used to calculate the position of the peaks measured at 11 different ψ angles. Absorption, background, and Lorentz–polarization corrections were applied before obtaining peak positions. The contribution of the $k\alpha_2$ radiation was also eliminated for calculations. In order to account for the elastic anisotropy of the diffracting crystallites, an anisotropy factor ARX=1.49 was chosen

Table 3 Measurement parameters of residual stresses by X-ray diffraction

Voltage 40 kV
Intensity 40 mA
Pinhole 2 mm
Detector slit 2 mm
Kβ Filter V
2θ measurement range 150–162°
Step 0.1
Time per step 3 s

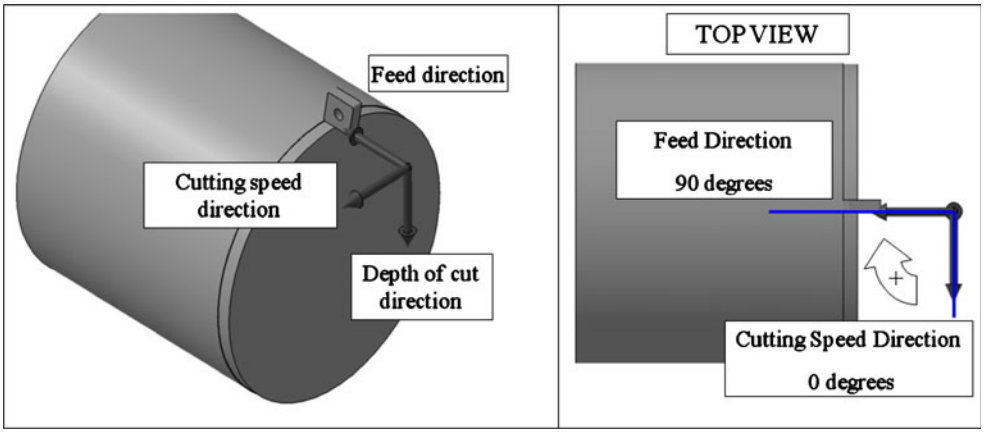

Fig. 2 Turning operations carried out and definition of the angles for the measurements of residual stresses

according to the values reported by He [17] for Fe cubic-based materials. The values of the elastic constants used to calculate residual stresses were E=210 GPa and ν=0.3.

The measurements were taken along three different directions (Fig. 2): feed direction (longitudinal direction, ϕ=90°); cutting speed direction (circumferential direction, ϕ=0°); and an intermediate direction (ϕ=45°). The residual stresses measured at the three different directions were used to obtain the Mohr's circles, which are a method to depict the stress state of a point in a solid. This state is represented in a $\sigma-\tau$ space. In this work, Mohr's circle was used to calculate the principal (maximum and minimum) residual stresses and their direction.

A plane stress model was assumed to calculate Mohr's circle. In a plane stress model, the coordinates of the circle are

$$\left(\frac{\sigma_x+\sigma_y}{2},0\right) \tag{7}$$

for the center and

$$r=\sqrt{\left(\frac{\sigma_x-\sigma_y}{2}\right)^2+\tau_{xy}^2} \tag{8}$$

for its radius. So, in order to calculate the Mohr's circle, the following values (in terms of components of the stress tensor) are needed: $\sigma_x=\sigma_{11}$, $\sigma_y=\sigma_{22}$, and $\sigma_{xy}=\sigma_{12}$. These three unknown quantities can be obtained by measuring residual stress along three different ϕ directions and using Eq. 3. Once this system is solved, Mohr's circle can be depicted and used to know the magnitude of the maximum and minimum residual stress and their direction in the sample reference system.

Table 4 Input parameters (factors)

Level	Feedrate, f_n (mm/rev)	Cutting speed, v_c (m/min)
−1	0.075	200
−0.6	0.100	
−0.2	0.125	
0		255
0.2	0.150	
0.6	0.175	
1	0.200	300

4 Results and discussion

The objective of the experiments is to analyze the influence of the cutting conditions in the surface integrity (residual stresses and roughness) of the turned material, assessing the main parameters influencing the residual stresses after machining. The residual stress state is evaluated mainly by the maximum principal stress (σ_{MAX}), minimum principal stress (σ_{MIN}), and their directions. Also, the Mohr's circle parameters are used for the discussion. The surface roughness, R_a, (measured with a Mitutoyo Surface Tester) is also analyzed.

The experimental data have been analyzed using analysis of variance (ANOVA) with the software STATGRAPHICS [18]. This allows establishing the main parameters (factors) influencing the surface residual stresses. Table 4 shows the factors, i.e., the input parameters and their levels, while Table 5 shows the main responses analyzed. Table 6 shows

Table 5 Output variables

Output variables
Maximum principal stress (σ_{MAX}) [MPa]
Minimum principal stress (σ_{MIN}) [MPa]
Maximum principal stress angle (φ_{MAX}) [°]
Mohr's Circle radius (R) [MPa]
Roughness (R_a) [μm]

Table 6 Residual stress measurements and obtained data

f_n	v_c	σ_0	σ_{45}	σ_{90}	σ_{MAX}	σ_{MIN}	R	C	σ_{MAX}	σ_{MIN}	R_a
−1	−1	473	607	252	630	94	268	362	32	122	0.27
−0.6	−1	481	614	288	633	135	248	384	33	123	0.46
−0.2	−1	512	623	302	647	166	240	407	32	122	0.58
0.2	−1	547	626	350	651	245	203	448	30	120	0.91
0.6	−1	570	656	368	681	256	212	469	30	120	1.18
1	−1	593	654	381	684	289	197	487	28	118	1.51
−1	0.1	432	556	160	589	2	293	296	31	121	0.27
−0.6	0.1	460	573	242	598	103	247	351	31	121	0.41
−0.2	0.1	490	550	250	586	153	216	370	28	118	0.6
0.2	0.1	526	602	311	631	205	212	418	29	119	0.94
0.6	0.1	536	601	333	629	239	195	434	29	119	1.22
1	0.1	562	599	321	639	243	198	441	26	116	1.55
−1	1	361	479	127	506	−18	262	244	31	121	0.28
−0.6	1	375	453	155	482	47	217	265	29	119	0.46
−0.2	1	430	510	211	539	101	218	320	29	119	0.63
0.2	1	−16	14	254	557	158	199	358	29	119	0.97
0.6	1	469	519	277	547	198	174	373	28	118	1.4
1	1	483	524	306	551	237	156	394	27	117	1.9

the results obtained for the different factors and responses. Regarding the residual stresses, the values gathered in Table 6 are the mean values measured. The measurement errors range from 7 to 44 MPa, being the most frequent error around 25–30 MPa.

4.1 Maximum principal stress

As can be seen in the PARETO diagram in Fig. 3a, the main factors affecting the value of the maximum principal stress are v_c, f_n, and v_c^2, in order of importance. Table 7 shows that these factors have a P value below 0.05 indicating its influence in the response with a 95% confidence level. The f_n^2 has little influence, while the interaction $v_c \times f_n$ is not important, as can also be assessed from the parallel curves showed in the interaction plot (Fig. 3c).

The main effects plot (Fig. 3b) shows that v_c has more influence than f_n; this results in a wider field response in the Y-axis. The influence of v_c is a second-order effect, as can be noticed by the curved response.

The R^2 statistic indicates that the model explains 95.66% of the variability in σ_{MAX}.

The results show that as feed increases residual stresses tend to be more tensile whereas an increase in cutting speed reduces tensile stresses. An explanation for this behavior is that lower f_n results in reduced cutting temperature (what implies lower tensile stresses as has been mentioned in the introduction) due to thinner chip thickness and lower heat generation in the chip plastic deformation. The temperature increase with feed has been measured experimentally by Outeiro et al. [19]. On the other hand, higher v_c results in a more adiabatic process with heat going with the chip instead of remaining in the workpiece surface: as cutting speed increases heat penetration is lower due to the reduction of the time to propagate heat. This effect is well known, especially in high-speed cutting, that tends to be a nearly adiabatic process when cutting speed is high enough, leading to lower part heating and, therefore, to less tensile residual stresses. Therefore, if the objective is to reduce the maximum principal stress in order to improve the fatigue behavior of the component, a lower feed rate and a higher cutting speed must be employed.

4.2 Minimum principal stress

The PARETO diagram for the minimum stress (Fig. 4a) shows that the main factors affecting the value of the minimum principal stress are f_n, v_c, and f_n^2, in order of importance. Table 8 shows that these factors have a P value below 0.05 indicating its influence in the response with a 95% confidence level. The interaction $v_c \times f_n$ has little influence, while the v_c^2 is negligible.

The main effects plot (Fig. 4b) shows that f_n has more influence than v_c, as a result of the wider field response in the Y-axis. The influence of f_n is a second-order effect, as can be noticed by the curved response; however, the behavior is practically linear because the linear term has higher influence than the quadratic term.

The R^2 statistic indicates that the model explains 98.34% of the variability in σ_{MIN}.

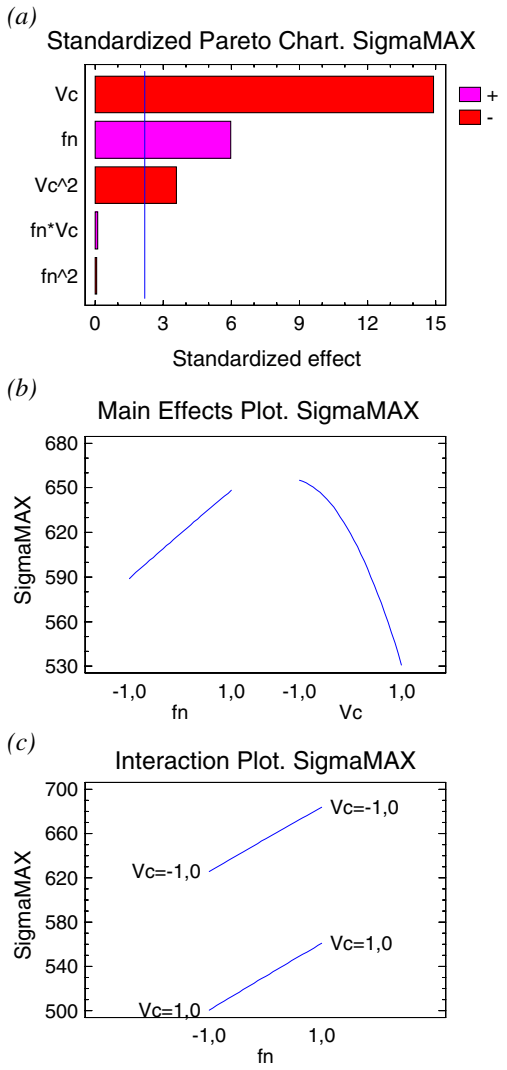

Fig. 3 Standardized Pareto chart (**a**), main effects plot (**b**), and interaction plot (**c**) for maximum principal stress (σ_{MAX})

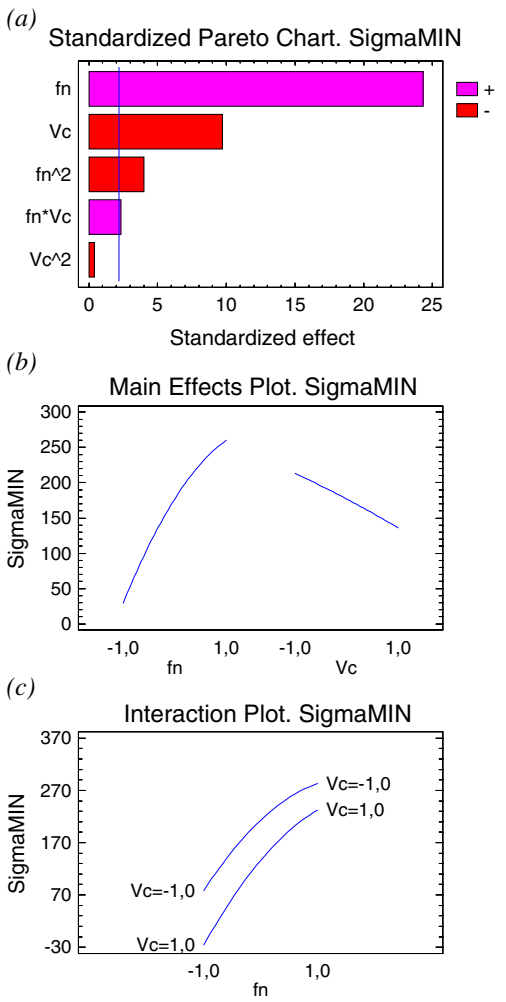

Fig. 4 Standardized Pareto chart (**a**), main effects plot (**b**), and interaction plot (**c**) for minimum principal stress (σ_{MIN})

Table 7 ANOVA table for maximum principal stress (σ_{MAX})

Factor	Sum of squares	Degrees of freedom	Mean square	*F* ratio	*P* value
f_n	7367.51	1	7367.51	35.35	0.0001
v_c	46154.0	1	46154.0	221.45	0.0000
f_n^2	0.492459	1	0.492459	0.00	0.9620
$f_n \times v_c$	1.79534	1	1.79534	0.01	0.9276
v_c^2	2646.71	1	2646.71	12.70	0.0039
Total error	2501.05	12	208.421		
Total (corrected)	57577.5	17			
R^2	95.66%				

The minimum principal stress can be reduced using a low feed rate and a high cutting speed, as occurs in the maximum principal stress analysis, so the same explanation of the previous paragraph remains valid for this case.

4.3 Maximum principal stress angle

Figure 5 shows the results for the angle of the maximum principal stress.

The minimum principal stress angle (ϕ_{MIN}) is obtained by adding 90° to the maximum principal stress angle (ϕ_{MAX}).

The angle of the maximum principal stress was found to be between 27° and 32° depending on the cutting conditions.

The PARETO diagram (Fig. 5a) shows that this angle basically depends on f_n and v_c. Table 9 shows that these factors have a *P* value below 0.05 indicating its influence in the response with a 95% confidence level. The most

Table 8 ANOVA table for minimum principal stress (σ_{MIN})

Factor	Sum of squares	Degrees of freedom	Mean square	*F* ratio	*P* value
f_n	111893.0	1	111893.0	589.09	0.0000
v_c	17847.9	1	17847.9	93.96	0.0000
f_n^2	2988.81	1	2988.81	15.74	0.0019
$f_n \times v_c$	1020.19	1	1020.19	5.37	0.0389
v_c^2	25.7696	1	25.7696	0.14	0.7190
Total error	2279.32	12	2279.32		
Total (corr.)	137096.0	17	189.943		
R^2	98.34				

Table 9 ANOVA table for maximum principal stress angle (ϕ_{MAX})

Factor	Sum of squares	Degrees of freedom	Mean square	*F* ratio	*P* value
f_n	35.071	1	35.071	40.25	0.0000
v_c	11.1169	1	11.1169	12.76	0.0038
f_n^2	0.340268	1	0.340268	0.39	0.5437
$f_n \times v_c$	0.179524	1	0.179524	0.21	0.6580
v_c^2	3.39578	1	3.39578	3.90	0.0718
Total error	10.4564	12	0.871369		
Total (corr.)	61.1727	17			
R^2	82.91%				

important conclusion is that the highest stress direction tends to the cutting speed direction as f_n and v_c increase, f_n being slightly more important than v_c.

The R^2 statistic indicates that the model explains 82.91% of the variability in ϕ_{MAX}.

The maximum principal stress angle near 0° (cutting speed direction ≡ tangential direction) is more favorable than near 90° (feed direction ≡ longitudinal direction) when a rotating shaft or a component is loaded under cyclic bending load, which can occur due to imbalance or misalignment.

4.4 Mohr's circle radius

The Mohr's circle radius is half the difference between the principal stresses values; therefore, it represents the

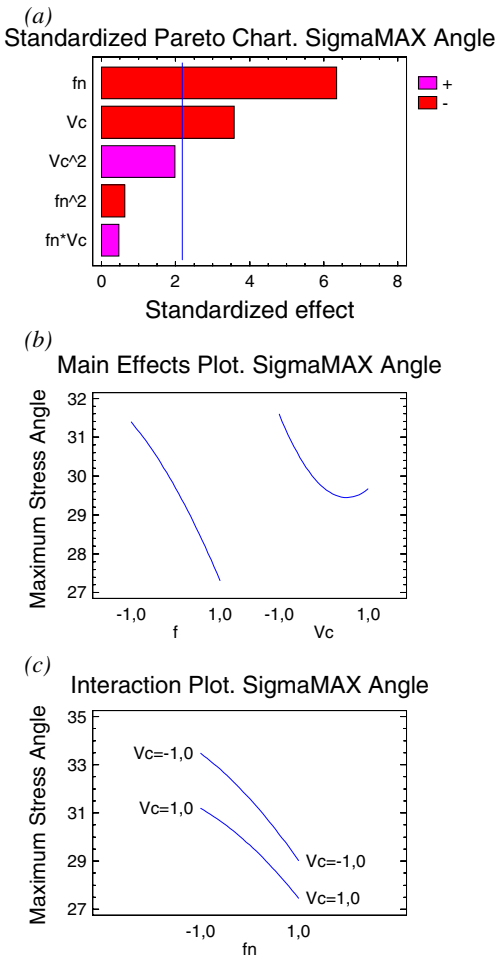

Fig. 5 Standardized Pareto chart (**a**), main effects plot (**b**) and Interaction Plot (**c**) for maximum principal stress angle (ϕ_{MAX})

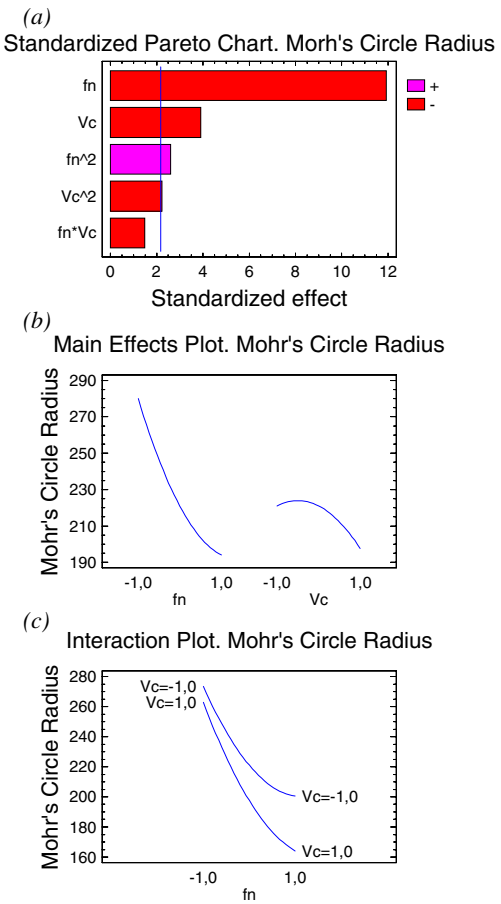

Fig. 6 Standardized Pareto chart (**a**), main effects plot (**b**), and interaction plot (**c**) for Mohr's circle radius (*R*)

Table 10 ANOVA table for Mohr's circle radius (R)

Factor	Sum of squares	Degrees of freedom	Mean square	F ratio	P value
f_n	15459.2	1	15459.2	141.99	0.0000
v_c	1649.94	1	1649.94	15.15	0.0021
f_n^2	728.144	1	728.144	6.69	0.0238
$f_n \times v_c$	234.097	1	234.097	2.15	0.1683
v_c^2	537.539	1	537.539	4.94	0.0463
Total error	1306.47	12	108.873		
Total (corr.)	19995.1	17			
R^2	93.47%				

homogeneity of the tensional state of the component. In Fig. 6, it can be noticed that the radius of the circle decreases as the values of f_n and v_c increase. In this case, obtaining more homogeneous stress state results in higher stress values, as can be assessed from the analysis of the maximum and minimum principal stresses.

In a general case study, the most favorable situation, i.e., lower tensile residual stress, is a result of using low f_n and high v_c; this involves a higher difference between the maximum and minimum stress, leading to less homogeneity in the stress state.

Table 10 shows the results of the ANOVA, indicating that the factors with P value below 0.05 have a significant influence in the response, Mohr's circle radius (R), with a 95% confidence level. The R^2 statistic indicates that the model explains 93.47% of the variability in radius.

4.5 Surface roughness

The main factor influencing the surface roughness is f_n, as already known due to the geometrical relations between the feed, the nose radius, and the roughness in turning operations according to AB Sandvik Coromant [20].

Table 11 ANOVA table for surface roughness (Ra)

Factor	Sum of squares	Degrees of freedom	Mean square	F ratio	P value
f_n	3.99663	1	3.99663	1464.84	0.0000
v_c	0.0444083	1	0.0444083	16.28	0.0017
f_n^2	0.109375	1	0.109375	40.09	0.0000
$f_n \times v_c$	0.0450778	1	0.0450778	16.52	0.0016
v_c^2	0.0114465	1	0.0114465	4.20	0.0631
Total error	0.0327405	12	0.00272837		
Total (corr.)	4.2786	17			
R^2	99.23%				

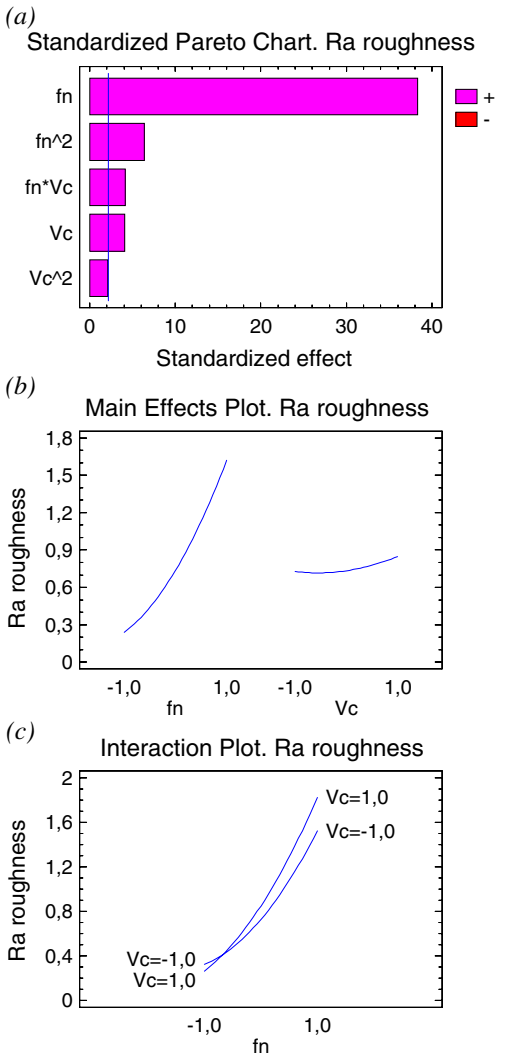

Fig. 7 Standardized Pareto chart (**a**), main effects plot (**b**), and interaction plot (**c**) for roughness (R_a)

However, in real machining operations other cutting parameters also influence the surface roughness because of the material behavior under large deformations. Thiele and Melkote [21] and Capello et al. [22] have also observed an increase on surface roughness with cutting speed and feed, respectively. In this case, it can be noticed that v_c and the interaction $f_n \times v_c$ are significant but have small influence in the R_a value compared to f_n. Therefore, it can be concluded that the main factor affecting R_a is f_n, having a second order influence. Table 11 shows the results of the ANOVA, indicating that the factors with P value below 0.05 have a significant influence in the response with a 95% confidence level. The R^2 statistic indicates that the model explains 99.23% of the variability in radius.

In a general case study, the most favorable situation, i.e., lower R_a, is a result of using low f_n and low v_c (Fig. 7).

5 Conclusions and future work

In this study, an assessment of the influence of the cutting conditions in the residual stresses and their direction was carried out. The analysis has been done using ANOVA, identifying the most relevant factors and their relative importance.

The surface integrity of a component is a result of the finishing machining operation, and it is characterized by the surface roughness and residual stress. The study shows that the optimum (less tensile) surface residual stress state is obtained using low feed rate (f_n) and high cutting speed (v_c), although this leads to a less homogeneous stress state. The reduction of the residual stresses when reducing feed rate is associated to a reduction of the heat generated during the machining process (heating of the parts during cutting favors the formation of tensile residual stresses). When increasing the cutting speed, the process is more adiabatic (less heating of the part, because heat is evacuated through the chip) what also leads to less tensile stresses. The low feed rate also leads to a good surface finishing (lower roughness), meeting both requirements (lower roughness and less tensile residual stresses) in a finished component.

The maximum stress direction has been found to lie between 27° and 32° from the cutting speed direction. An influence of the cutting parameters on the maximum stress direction was also found. Although the influence is small, it was found that changes in cutting parameters leads to a variation in the maximum stress angle which tends to be closer to the cutting speed direction when cutting speed and feed rate increases.

The future work includes the identification of the influence of the tool geometry in the value and direction of the surface residual stress. The main parameters to be studied are the nose radius, the rake angle, the position angle, and the inclination angle.

Acknowledgements The authors thank to the Industrial Department of the Basque Government for the financial support of this work, which is part of the MANUFACTURING 0,0 project developed under the ETORTEK program. The authors also thank to the CIC marGUNE for the access to their X-ray diffractometer to perform the residual stress measurements.

References

1. Schwach DW, Guo YB (2005) Feasibility of producing optimal surface integrity by process design in hard turning. Mat Sci Eng A 395:116–123
2. Withers PJ, Bhadeshia HKDH (2001) Residual stress part 2 – nature and origins. Mat Sci Tech 17:366–375
3. Griffiths B (2001) Manufacturing surface technology—surface integrity & functional performance: Manufacturing engineering modular series. Taylor & Francis, New York
4. Wyatt JE, Berry JT (2006) A new technique for the determination of superficial residual stresses associated with machining and other manufacturing processes. J Mater Process Technol 171:132–140
5. Capello E (2005) Residual stress in turning - part I: influence of process parameters. J Mater Process Technol 160:221–228
6. M'Saoubi R, Outeiro JC, Changeux B, Lebrun JL, Morao Dias S (1999) Residual stress analysis in orthogonal machining of standard and resulfurized AISI 316 L steels. J Mater Process Technol 96:225–233
7. Outeiro JC, Dias AM, Lebrun JL, Astakhov VP (2002) Machining residual stresses in AISI 316 L steel and their correlation with the cutting parameters. Mach Sci Technol 6(2):251–270
8. Jang DY, Watkins TR, Kozaczek KJ, Hubbard CR, Cavin OB (1996) Surface residual stresses in machined austenitic stainless steel. Wear 194:168–173
9. Gunnberg F, Escursell M, Jacobson M (2006) The influence of cutting parameters on residual stresses and surface topography during hard turning of 18MnCr5 case carburized steel. J Mater Process Technol 174:82–90
10. Pink J (1996). Landing gear structural integrity. Aersospace engineering. March. 13–16
11. AISI 4340 General Information. http://www.efunda.com/materials
12. ASM International (1990) Carbon and low alloy steels in metals handbook vol 1: properties and selection: iron, steels and high performance alloys, 10th edn. ASM International, Almere
13. Dahlman P, Gunnberg F, Jacobson M (2004) The influence of rake angle, cutting feed and cutting depth on residual stresses in hard turning. J Mater Process Technol 147(2):181–184
14. Chou YK, Evans CJ, Barash MM (2003) Experimental investigation on cubic boron nitride turning of hardened AISI 52100 steel. J Mater Process Technol 134(1):1–9
15. Lu J (1996) Handbook of measurement of residual stresses. Fairmont, Lilburn
16. Noyan IC, Cohen JB (1987) Residual stress: measurement by diffraction and interpretation. Springer, New York
17. He BB (2009) Two dimesional X-ray diffraction. Wiley, Chichester, 258 pp
18. STATGRAPHICS software and documentation. http://www.statgraphics.com
19. Outeiro JC, Dias AM, Lebrun JL (2004) Experimental assessment of temperature distribution in three-dimensional cutting process. Mach Sci Technol 8(3):357–376
20. AB Sandvik Coromant (2005) "Guía Técnica de mecanizado – Manual de Sandvik Coromant". AB Sandvik Coromant, C-2900:3 SPA/01.
21. Thiele JD, Melkote SN (1999) Effect of cutting edge geometry and workpiece hardness on surface generation in the finish hard turning of AISI 52100 steel. J Mater Process Technol 94(2–3):216–226
22. Capello E, Davoli P, Bassanini G, Bisi A (1999) Residual stresses and surface roughness in turning. J Eng Mat Tech – ASME Trans 121(3):346–351